MARTIN MARIETTA ENERGY SYSTEMS LIBRARIES
3 4456 0050580 7

106

CENTRAL RESEARCH LIBRARY
DOCUMENT COLLECTION

ORNL-2939
UC-80 - Reactors-General

EFFECT OF HEAT FLUX ON THE CORROSION OF ALUMINUM BY WATER

PART I. EXPERIMENTAL EQUIPMENT AND PRELIMINARY TEST RESULTS

J. C. Griess
H. C. Savage
T. H. Mauney
J. L. English

CENTRAL RESEARCH LIBRARY
DOCUMENT COLLECTION
LIBRARY LOAN COPY
DO NOT TRANSFER TO ANOTHER PERSON
If you wish someone else to see this document, send in name with document and the library will arrange a loan.

OAK RIDGE NATIONAL LABORATORY
operated by
UNION CARBIDE CORPORATION
for the
U.S. ATOMIC ENERGY COMMISSION

Printed in USA. Price $1.50. Available from the
Office of Technical Services
Department of Commerce
Washington 25, D.C.

LEGAL NOTICE

This report was prepared as an account of Government sponsored work. Neither the United States, nor the Commission, nor any person acting on behalf of the Commission:

A. Makes any warranty or representation, expressed or implied, with respect to the accuracy, completeness, or usefulness of the information contained in this report, or that the use of any information, apparatus, method, or process disclosed in this report may not infringe privately owned rights; or

B. Assumes any liabilities with respect to the use of, or for damages resulting from the use of any information, apparatus, method, or process disclosed in this report.

As used in the above, "person acting on behalf of the Commission" includes any employee or contractor of the Commission, or employee of such contractor, to the extent that such employee or contractor of the Commission, or employee of such contractor prepares, disseminates, or provides access to, any information pursuant to his employment or contract with the Commission, or his employment with such contractor.

ORNL-2939
Reactors - General

Contract No. W-7405-eng-26

REACTOR EXPERIMENTAL ENGINEERING DIVISION

EFFECT OF HEAT FLUX ON THE CORROSION OF ALUMINUM BY WATER

PART I. EXPERIMENTAL EQUIPMENT AND PRELIMINARY TEST RESULTS

J. C. Griess, H. C. Savage, T. H. Mauney, and J. L. English

DATE ISSUED

APR 29 1960

OAK RIDGE NATIONAL LABORATORY
Oak Ridge, Tennessee
operated by
UNION CARBIDE CORPORATION
for the
U. S. ATOMIC ENERGY COMMISSION

MARTIN MARIETTA ENERGY SYSTEMS LIBRARIES
3 4456 0050580 7

CONTENTS

	Page
ABSTRACT	1
INTRODUCTION	1
TEST EQUIPMENT AND CONDITIONS	3
Test Specimen	4
Electrical Power Supply	8
Pump Loop	10
Operation Procedure and Test Conditions	10
RESULTS	15
Data Acquired During the Test	15
Specimen Temperature	15
Water Chemistry	20
Heat Balance	21
Specimen Examination	21
Change in Electrical Resistance	21
Visual Examination	22
Specimen Thickness and Surface Roughness	29
Determination of Oxide Thickness	29
Metallographic Examination	31
DISCUSSION	38
ACKNOWLEDGMENTS	43
REFERENCES	43

EFFECT OF HEAT FLUX ON THE CORROSION OF ALUMINUM BY WATER
PART I. EXPERIMENTAL EQUIPMENT AND PRELIMINARY TEST RESULTS

J. C. Griess, H. C. Savage, T. H. Mauney, and J. L. English

ABSTRACT

An experiment designed to determine the effect of heat flux on the corrosion of 1100 aluminum by water under conditions simulating those that will exist in the High-Flux Isotope Reactor has been carried out. The passage of an a-c current through the test specimen heated the specimen, and a flow of water from a bypass line of a pump loop provided cooling. Water flowing at 33 fps entered a coolant channel in the specimen at 155°F and was heated to 192°F on passing through the specimen. Heat fluxes of 0.50×10^6 and 1.62×10^6 Btu/hr·ft^2 on different parts of the specimen were constant during the 10-day test. The formation of adherent corrosion products on the coolant surfaces resulted in increasing aluminum temperatures as the test progressed. During the 10-day test the maximum temperature increase occurred at the coolant outlet and amounted to 189°F. In this region an adherent, nearly transparent, corrosion-product layer about 0.002 in. thick formed; the aluminum was penetrated to a depth of 0.007 in., 0.005 in. of which was intergranular in nature.

The results of this test indicate that the temperature of the aluminum cladding on the fuel elements of the High-Flux Isotope Reactor will be higher than calculated, assuming clean aluminum surfaces, and that the extent of corrosion must be reduced either by the addition of inhibitors to the water or by the use of an alloy more corrosion resistant than 1100 aluminum.

INTRODUCTION

The corrosion of aluminum and its alloys in water has been extensively investigated, and many papers concerning their corrosion resistance appear in the literature.[1-6] However, only a few studies have been reported on the effect of heat flux on the corrosion of aluminum in

aqueous systems.[3,7] From the existing data it appears that the major effect of heat flux on the corrosion of aluminum is to raise the surface temperature, which causes an increase in corrosion rate. As corrosion proceeds, the formation of a surface layer of corrosion products of low thermal conductivity results in an additional increase in the aluminum temperature and a further increase in corrosion rate.

Aluminum-clad fuel elements have been used successfully for years in water-cooled research reactors, but in these cases the water temperature and heat flux are so low that the surface temperature of the aluminum remains relatively low, and corrosion is not a major problem. At very high heat fluxes, even with low coolant temperature, the surface temperature of the aluminum can become high enough so that corrosion can be of major concern. Such high heat fluxes will exist in the High-Flux Isotope Reactor which is currently being designed at Oak Ridge National Laboratory.

The High-Flux Isotope Reactor has as its objective the production of transplutonium elements. A preliminary design report has been written,[8] and the reader is referred to this report for design details. For the purpose of this report it is sufficient to note that thin fuel plates with a 0.010-in. clad of aluminum will be used and that heat fluxes as high as 1.5×10^6 Btu/hr·ft^2 will exist. The fuel will consist of a uranium-aluminum alloy and/or a dispersion of U_3O_8 in aluminum. The coolant channels between the plates will be 0.050 in. The water will enter the reactor core at 120°F and will leave at 190°F at a flow rate of 40 fps. Considering hot-spot and hot-channel factors, and assuming no corrosion products on the aluminum, a maximum surface temperature of 388°F is calculated. Because of the high power density, each reactor

fuel loading will last only 10 days, and as a result corrosion rates much higher than could be considered in research or power reactors can be tolerated.

In a reactor utilizing thin fuel plates with high heat fluxes and high-velocity water flowing past them, the mechanical strength of the plates becomes a problem. This fact is especially true with aluminum, which has low strength even at room temperature and which loses its strength rapidly as the temperature increases. For example, the yield strength of 1100 aluminum is nominally 5000 psi at room temperature and only 2000 psi at 500°F. Thus, apart from corrosion, it is necessary to know the temperature of the fuel plates for design purposes.

It is the purpose of this report to describe the equipment used to conduct experiments on the effect of heat flux on the corrosion of aluminum and to present the results of the first test. Obviously no complete discussion on the effect of heat transfer on corrosion can be made on the basis of one test, but the preliminary results appear significant enough to justify presentation at this time.

TEST EQUIPMENT AND CONDITIONS

The determination of the effect of heat flux on the corrosion of a material requires a means of supplying heat to the test material and a means of continuously removing the heat. For the test described here, an electric current was passed through the test specimen to generate heat, and a conventional test loop was used to provide a flow of cooling water for heat removal. The aluminum test specimen, which contained a coolant channel, was mounted in a bypass line of a pump loop, and water flowing through the channel removed the heat. The test equipment was

designed so that corrosion could be studied at heat fluxes of at least 1.5×10^6 Btu/hr·ft^2.

The following sections describe the equipment and test conditions. While these conditions are specific for the test described here, it should be noted that the equipment is capable of operation over wide ranges of specimen heat fluxes and coolant temperature, pressure, and flow rates.

Test Specimen

A photograph of the corrosion test specimen and diagrams of its cross-sectional areas are shown in Fig. 1. The over-all length of the specimen was 8.5 in.; a 1-in. length at each end was used to weld the specimen to the electrodes, leaving a heated length of 6.5 in. The dimensions of the rectangular-shaped coolant channel were 0.500 in. by 0.050 in. The 0.050-in. dimension was designed to be the same as that of the cooling channel between fuel plates in the High-Flux Isotope Reactor. Due to improper fit of the backup plates (described later), internal pressure expanded the channel gap to 0.058 in. during the test. The cross-sectional metal area of the 6.5-in.-long heated portion was designed so that 80% of the total electric-resistance heat would be generated in the 0.100-in.-thick x 0.300-in.-wide center sections and 20% in the 0.025-in.-thick side sections. With these dimensions the ratio of heat flux across the surface under the 0.100-in.-thick surface to that under the 0.025-in.-thick surface is 3.3. The heating load was distributed in this manner to prevent burnout at the extremities of the flow channel where it was expected that heat-transfer coefficients might be low.

UNCLASSIFIED
ORNL-LR-DWG. 47281

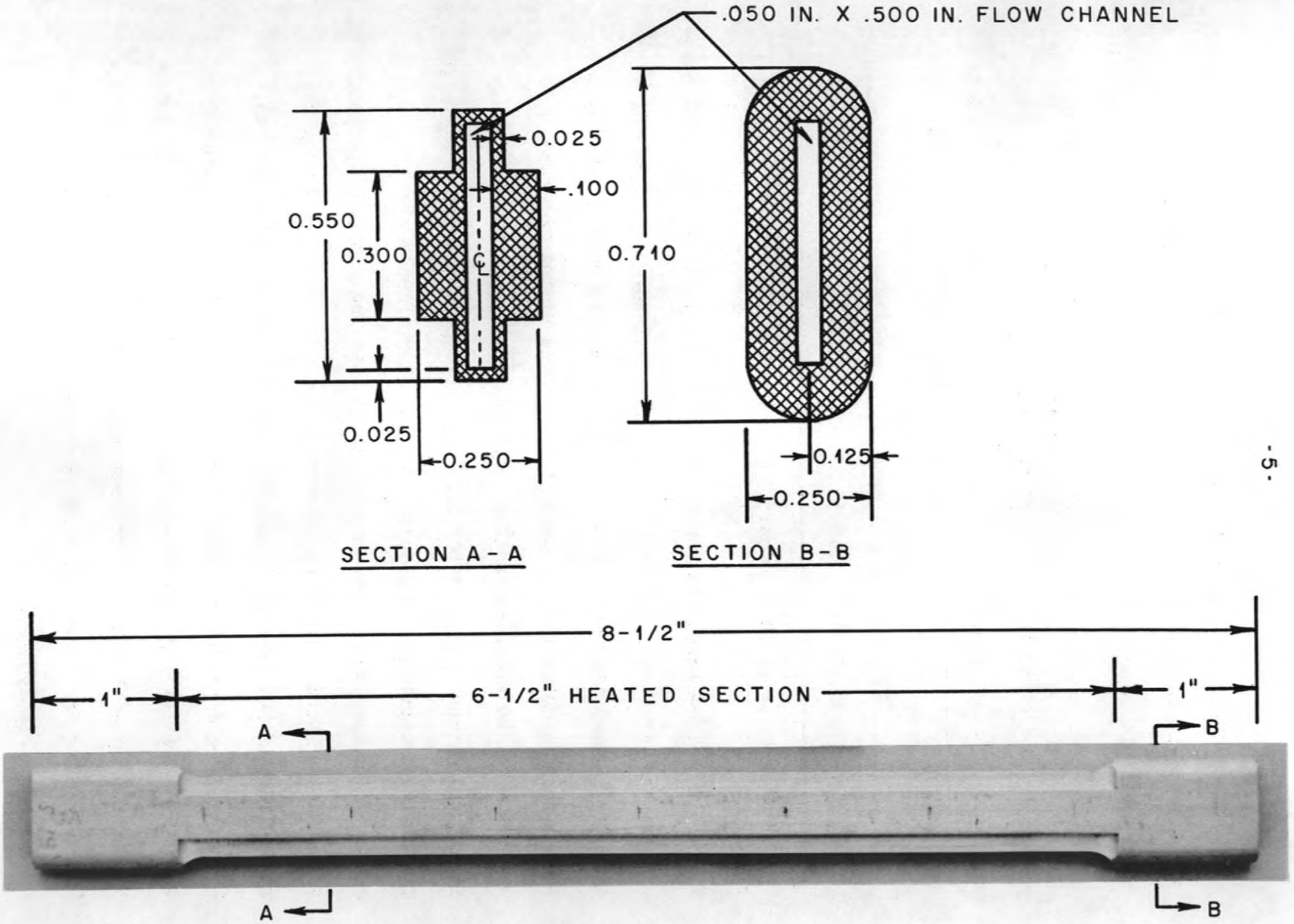

Fig. 1. Aluminum Corrosion Test Specimen.

Aluminum rod stock of type 1100 aluminum was used to fabricate the initial specimen. The chemical composition of the aluminum used is shown in Table 1.

Table 1. Chemical Composition of the Aluminum Test Specimens

Element:	Cr	Cu	Fe	Mg	Ni	Si	Sn	Al
Wt %	<0.05	0.11*	0.50*	<0.01	<0.02	0.1	<0.02	>99

* Chemically determined; others spectrographically determined.

After the rod was bored and reamed to dimensions suitable for final shaping, it was annealed for 1 hr at 650°F. The approximate dimensions of the flow channel were obtained by pressing the tube onto a mandrel, and the final dimensions were obtained by drawing a sizing die through the test piece. The specimen was then machined to provide the 0.025-in.-thick webs on each side. After forming, the specimen was degreased in acetone. No other cleaning operations were performed.

The aluminum test specimen was welded into the massive electrodes as shown in Fig. 2. The large electrodes were necessary both for the attachment of the power leads and to make leak-tight connections to flanges in the loop bypass line. Four stay bolts rigidly supported the electrodes. After the specimen was welded to the electrodes, 12 thermocouples were spot-welded to the outer surface of the specimen so that temperatures along the length could be measured during the test (see Fig. 6 for thermocouple locations).

UNCLASSIFIED
ORNL-LR-DWG. 47282

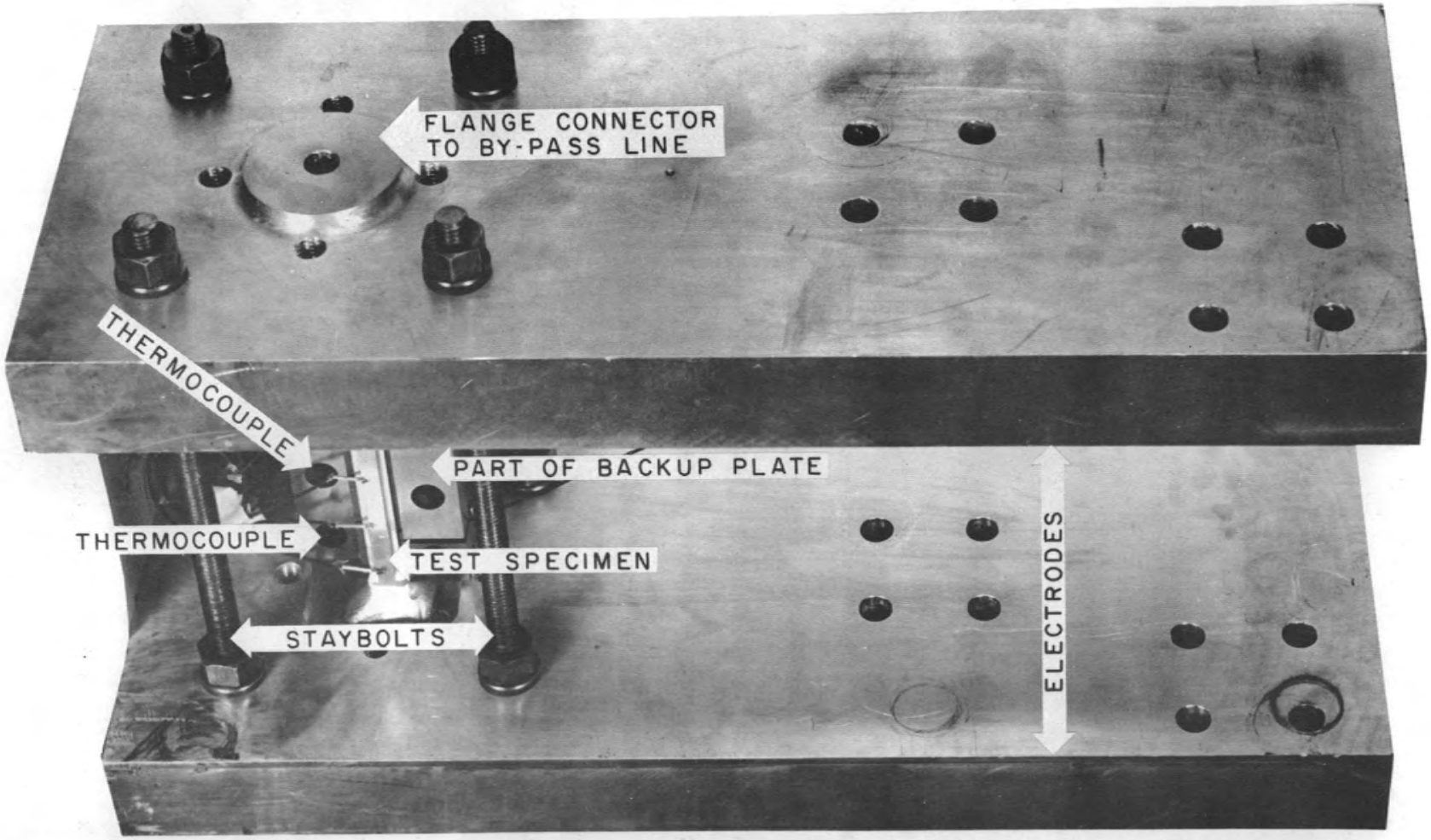

Fig. 2. Photograph of the Test Specimen Welded to the Electrodes.

With the thermocouples attached, close-fitting Mycalex (bonded mica and glass) pieces, which provided electrical and thermal insulation, were placed around the specimen. Stainless steel backup plates were bolted around the Mycalex so that internal pressures as high as 1000 psi could be used with the relatively thin aluminum test specimen. Details of the complete test assembly are shown in Fig. 3.

Electrical resistance of the 6.5-in.-long heated portion of the specimen between the electrodes was 1.10×10^{-4} ohm (room temperature), a value which compares favorably with the design value of 1.00×10^{-4} ohm. It was calculated that the resistance of the test piece would increase sufficiently, at an assumed average aluminum temperature of 170°C during operation, to produce the desired heat flux when 10,000 amps of current were passed through the specimen.

The metal cross-sectional area of the specimen was 5.20×10^{-4} ft^2 (4.16×10^{-4} ft^2 for the 0.100-in.-thick center section and 1.04×10^{-4} ft^2 for the 0.025-in.-thick edges). Corresponding cooling surface area for the 6.5-in.-long heated portion was 0.0496 ft^2, of which 0.0271 ft^2 was under the thick high-heat-flux section and 0.0225 ft^2 was under the edges (low heat flux).

Electrical Power Supply

A water-cooled transformer, with taps for step-wise adjustment of output, was used to supply approximately 10,000 amps of a-c current for specimen heating. At 10,000 amps current flow, and for the resistance of the specimen at an estimated average temperature of 170°C, 16.0 kw of heat would be generated in the test specimen; this is equivalent to 55,000 Btu/hr. Resultant heat fluxes across the water-cooled

UNCLASSIFIED
ORNL-LR-DWG. 47283

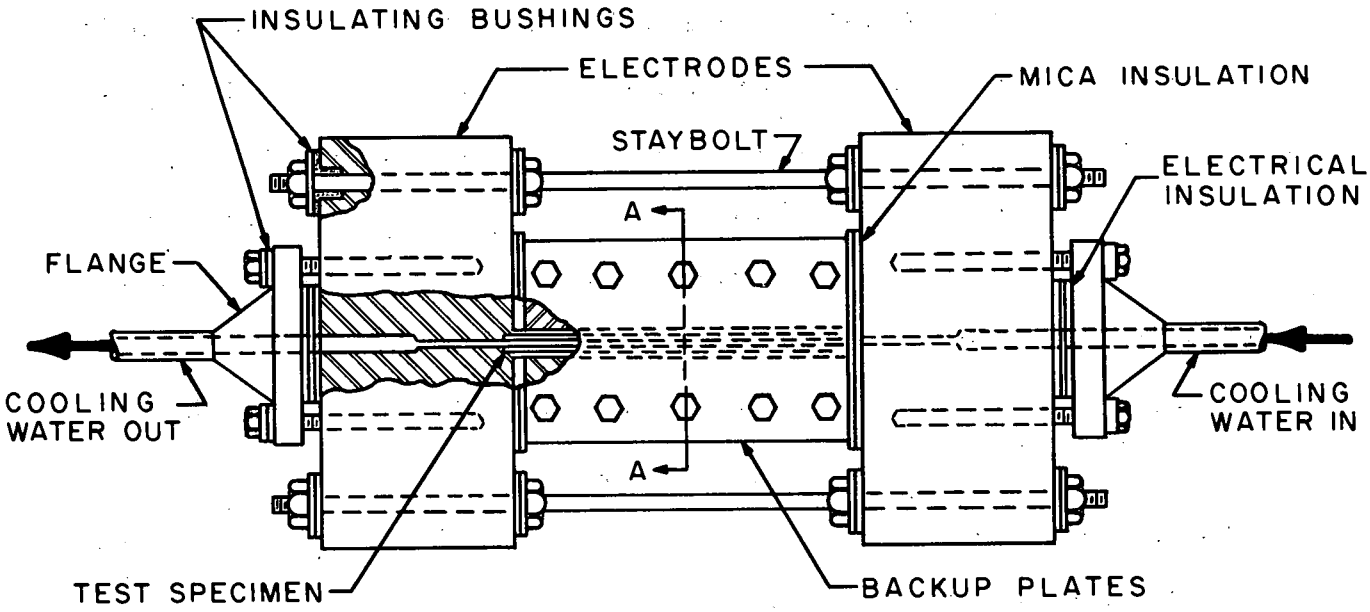

Top View
(No Scale)

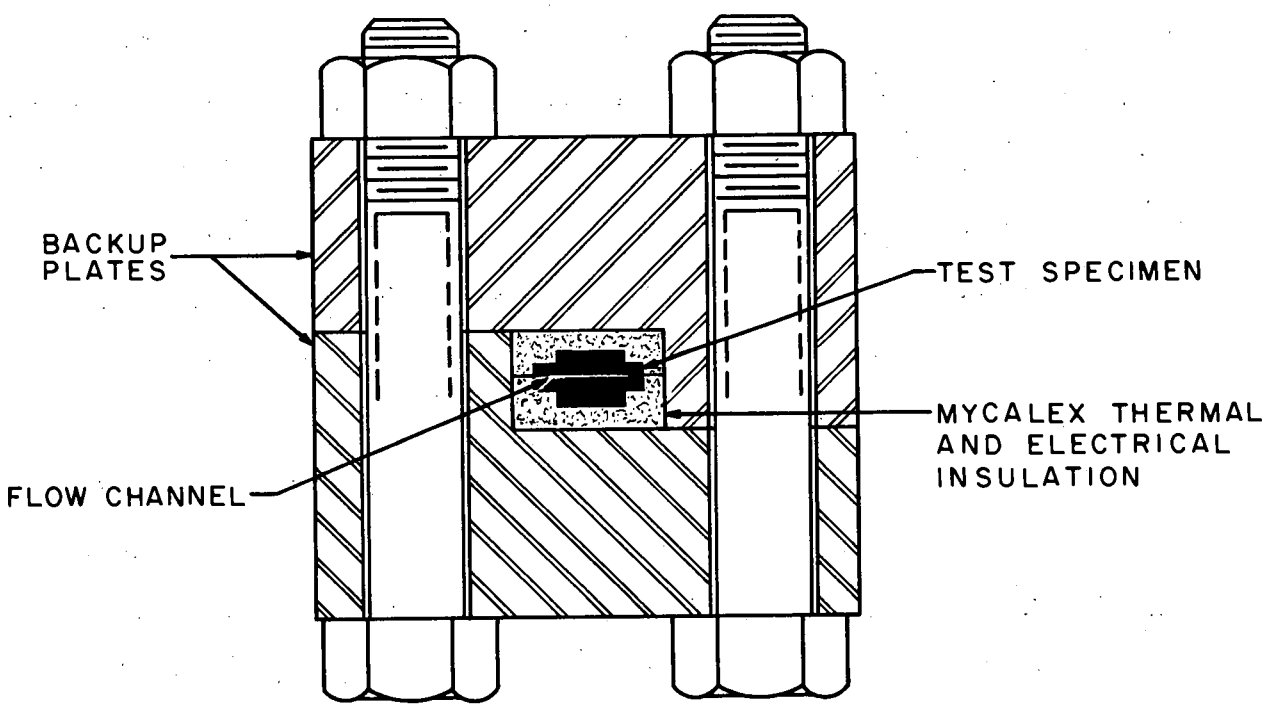

Section at A-A
(Full Size)

Fig. 3. Sketch of Complete Test Apparatus Assembly.

heat-transfer surface were calculated to be approximately 1.6×10^6 Btu/hr·ft^2 for the center section and approximately 0.50×10^6 Btu/hr·ft^2 for the edges.

Pump Loop

The pump loop in which the test specimen assembly was installed was designed for operation at temperatures to 300°C and pressures to 1500 psi. Temperature and pressure of the coolant can be individually controlled, as can the flow rate of the coolant through the specimen. The system pressure was regulated by means of a letdown valve and feed pump. Coolant flow through the test section was controlled by a throttling valve, and an indicator-recorder continuously monitors this flow rate. In this test a 0.13-gph bypass stream from the loop was cooled and passed through a mixed-bed ion exchanger to control the coolant-water purity. The loop is also equipped with sampling stations so that representative samples of the water may be removed from the main loop stream and from the discharge of the ion-exchange column.

Figure 4 is a schematic diagram of the pump loop, and Fig. 5 is a photograph of the test assembly as installed in the loop bypass line.

The loop is constructed throughout of type 347 stainless steel and has a volume of 5.8 gal. Stainless steel surface area exposed to the circulating water is 15.5 ft^2. In this test the total aluminum surface area exposed to the water was approximately 0.07 ft^2.

Operation Procedure and Test Conditions

After the specimen was installed, the system was filled with distilled water and hydrostatically pressure-tested at 500 psi to verify leak-tightness. The system pressure was adjusted to 300 psig by means

UNCLASSIFIED
ORNL-LR-DWG. 47284

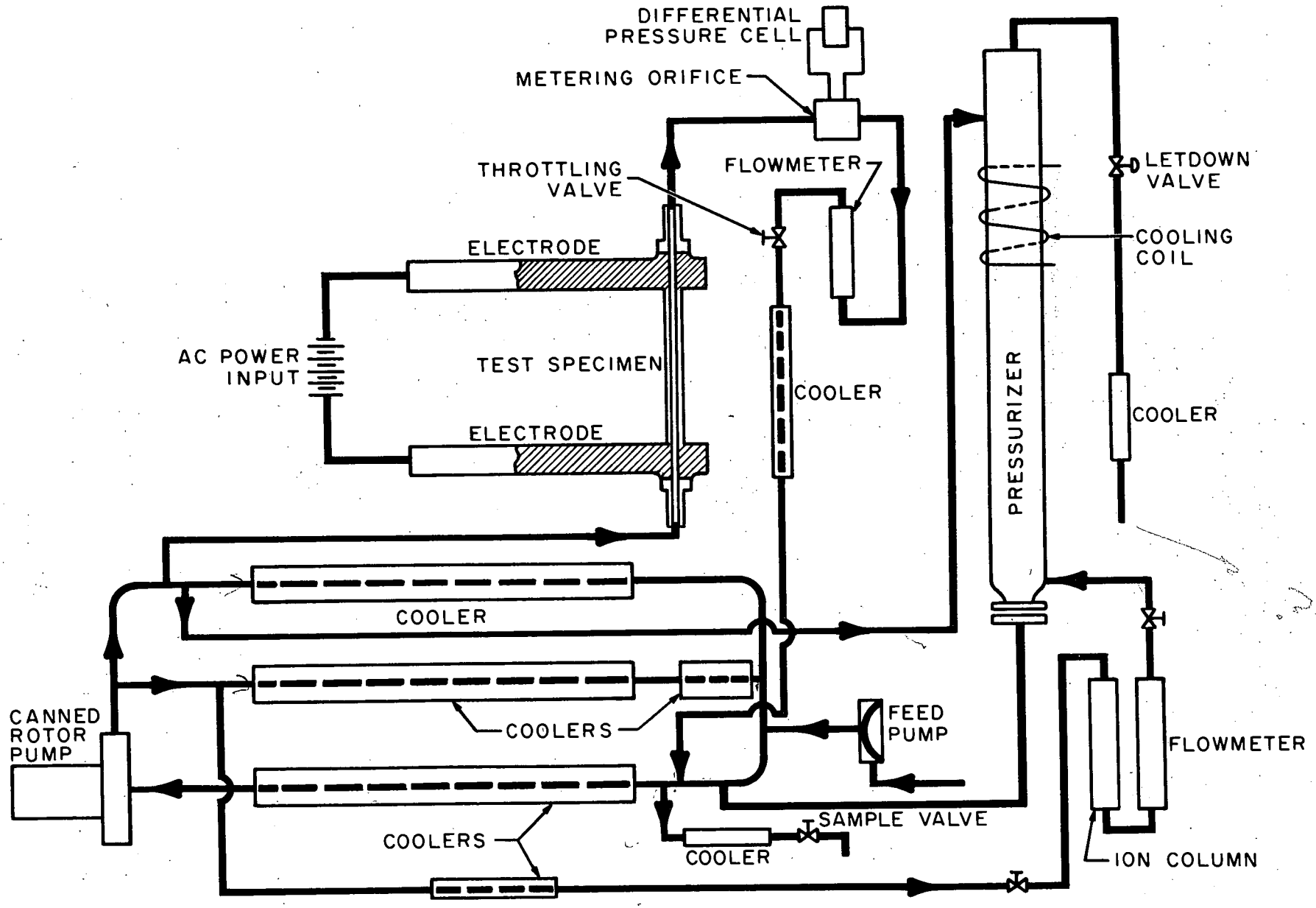

Fig. 4. Schematic Diagram of Pump Loop and Test Apparatus.

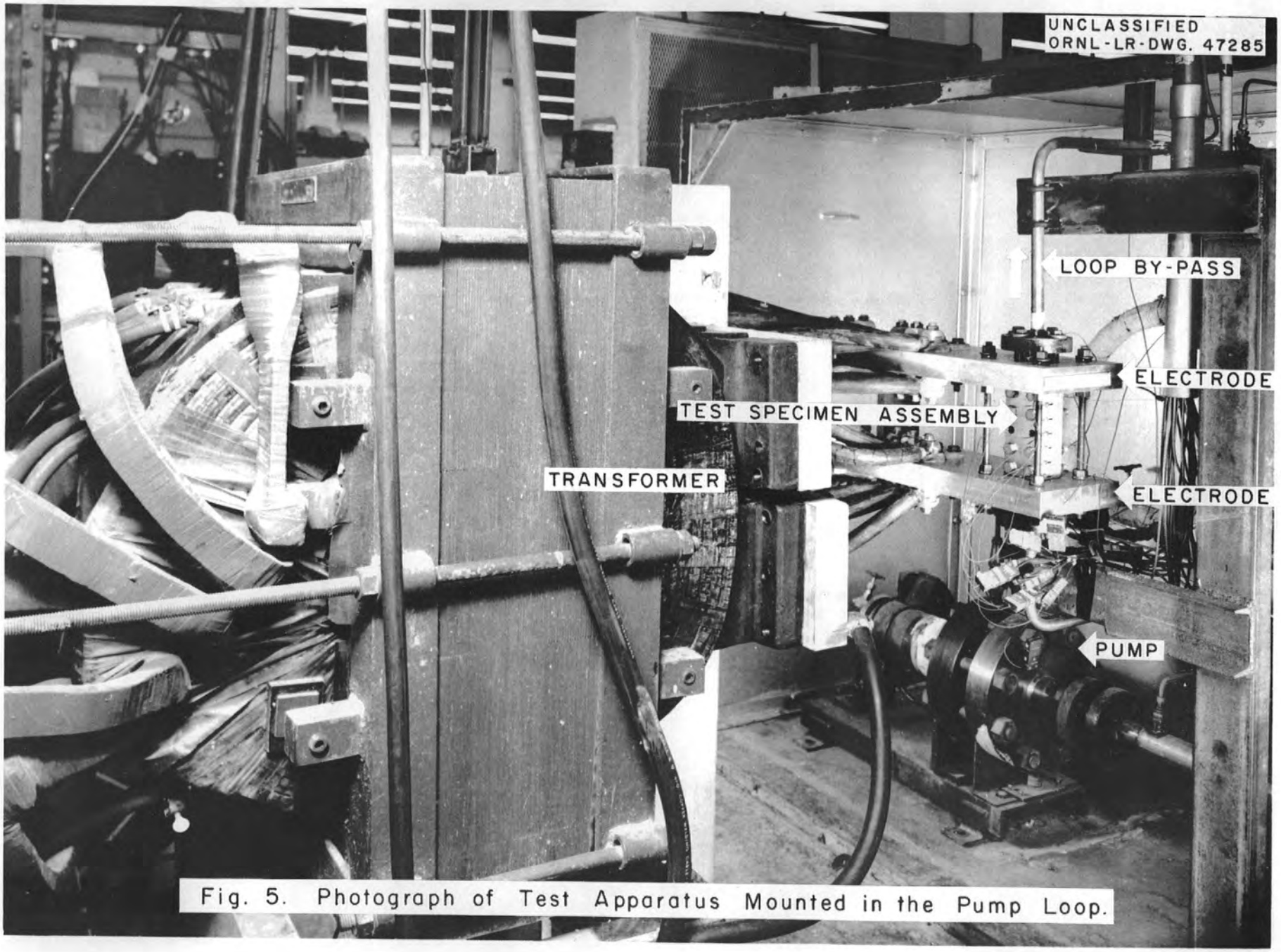

Fig. 5. Photograph of Test Apparatus Mounted in the Pump Loop.

of a high-pressure diaphragm feed pump and letdown valve, and the main loop circulating pump was turned on. Then the flow rate through the test specimen was adjusted by means of the regulating valve. Water let down from the loop was cooled and routed to a stainless steel tank, from which it was returned to the loop by means of the feed pump. This tank was continuously sparged with nitrogen to reduce the dissolved oxygen content of the water.

After the loop operating temperature was reached and after the conductivity and pH of the water indicated that the water purity was satisfactory, the power supply to the test specimen was turned on. Because of minor adjustments required on the loop and power-supply circuit in this initial experiment, some 2 hr were required before steady-state temperatures were reached in the loop main stream and in the test specimen.

Throughout the course of the 240-hr run the inlet and outlet temperatures of the coolant water and the temperatures on the outside metal surface of the test specimen were continuously recorded. Samples of the water were also regularly removed for examination.

Operating conditions for this initial test are summarized in Table 2. The test operation was continuous for 10 days (240 hr), which corresponds to the expected life of each fuel loading of the High-Flux Isotope Reactor.

Table 2. Summary of Test Conditions

Flow Rate	
Main loop stream	80 gpm
Test-specimen cooling channel	2.95 gpm (33 fps)
Letdown and feed	0.26 gpm
Ion-exchange column	0.13 gph
Pressures	
Specimen inlet	370-420 psia*
Pressure drop through specimen	25 psi
Temperatures	
Loop	155°F
Specimen inlet cooling water	155-157°F
Specimen outlet cooling water	191-193°F
Average cooling water Δt	37°F
Heat Generation**	
Specimen total	55,000 Btu/hr (16 kw) (190×10^6 Btu/hr·ft^3 or 2.0 kw/cm^3)
In 0.10-in.-thick center section	44,000 Btu/hr
In 0.025-in.-thick edges	11,000 Btu/hr
Heat Flux	
Flow-channel surface under 0.100-in.-thick section	1.62×10^6 Btu/hr·ft^2
Flow-channel surface at edges (0.025-in.-thick section)	0.50×10^6 Btu/hr·ft^2

* The pressure remained constant during the run. An uncertainty in the accuracy of the pressure gage is the reason for the range.

** Total heat generated in the specimen as calculated from measurements of current flow and voltage drop and that calculated from a heat balance of the cooling water (flow rate and temperature use) usually agreed to within ±5%.

RESULTS

Pertinent results were obtained both during the course of the test and upon examination of the specimen at the conclusion of the test. To facilitate reporting of the data, the results are divided into two sections: (1) observations made during the test and (2) postrun examination of the test specimen.

Data Acquired During the Test

Specimen Temperature

Throughout the test the temperatures at several locations on the outside of the specimen were continuously recorded. All thermocouples that functioned properly indicated that the temperature of the aluminum increased as the test progressed. Figure 6 shows the location of the thermocouples on the outside surface of the specimen. With the exception of thermocouples 3 and 5, which were located on the thin section of the aluminum, all were attached along the central axis of the specimen in the region of high heat flux. Figures 7, 8, and 9 show how the temperature at the thermocouple locations changed with time. Also shown on Fig. 9 is the temperature of the inlet and outlet water (thermocouples 1 and 2, respectively). Thermocouples 7 and 14 did not function properly, and their readings were not recorded. The temperatures plotted are thermocouple readings taken from the multipoint recorder at approximately 4-hr intervals. The fluctuations in the curves appear to be related to random changes in the electrical power input to the specimen, since the changes were reflected in all thermocouples simultaneously. The curves do not start from time zero because of difficulty at the start in loop temperature control, and as a result the inlet cooling-water temperature

UNCLASSIFIED
ORNL-LR-DWG. 47286

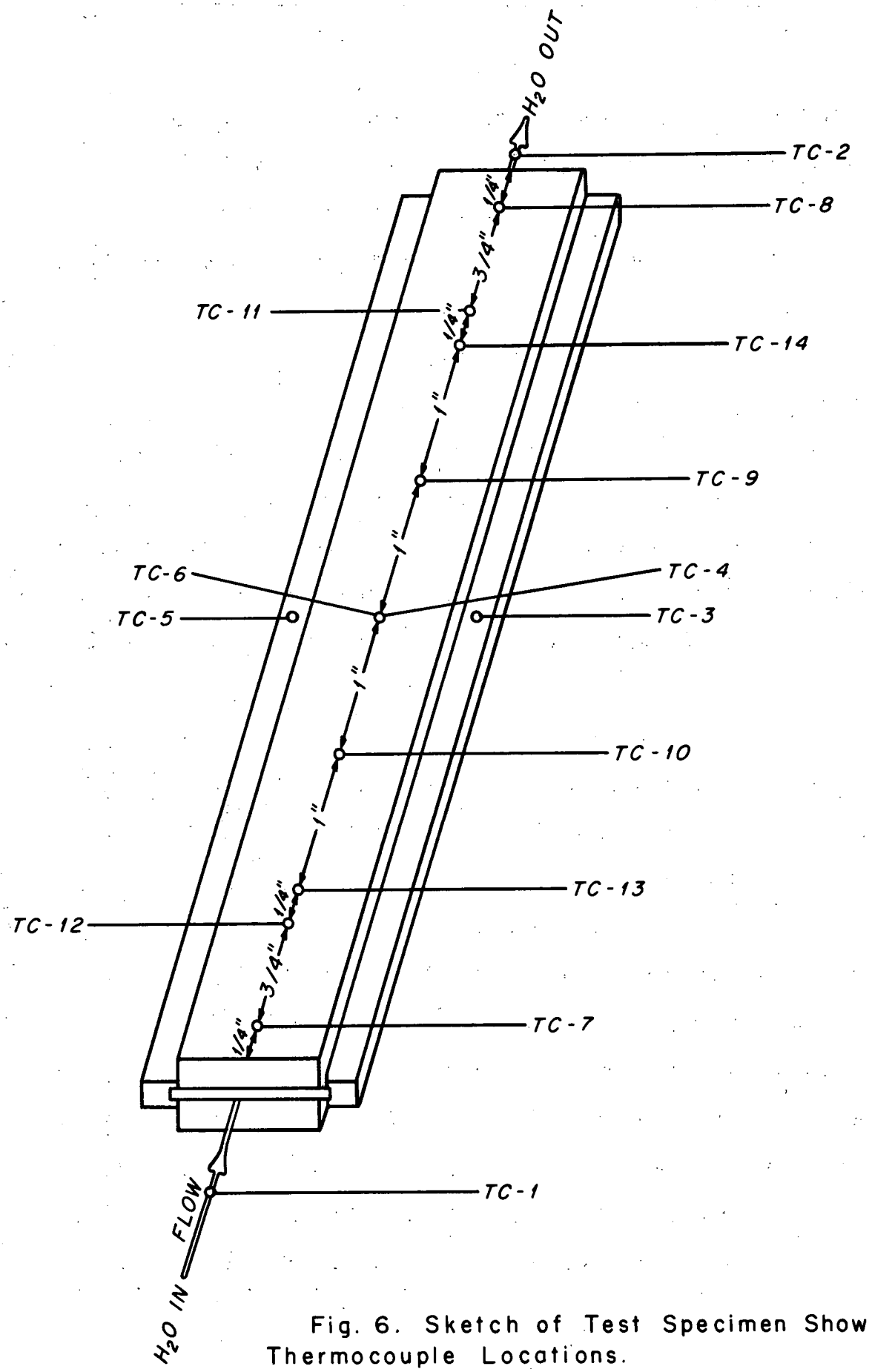

Fig. 6. Sketch of Test Specimen Showing Thermocouple Locations.

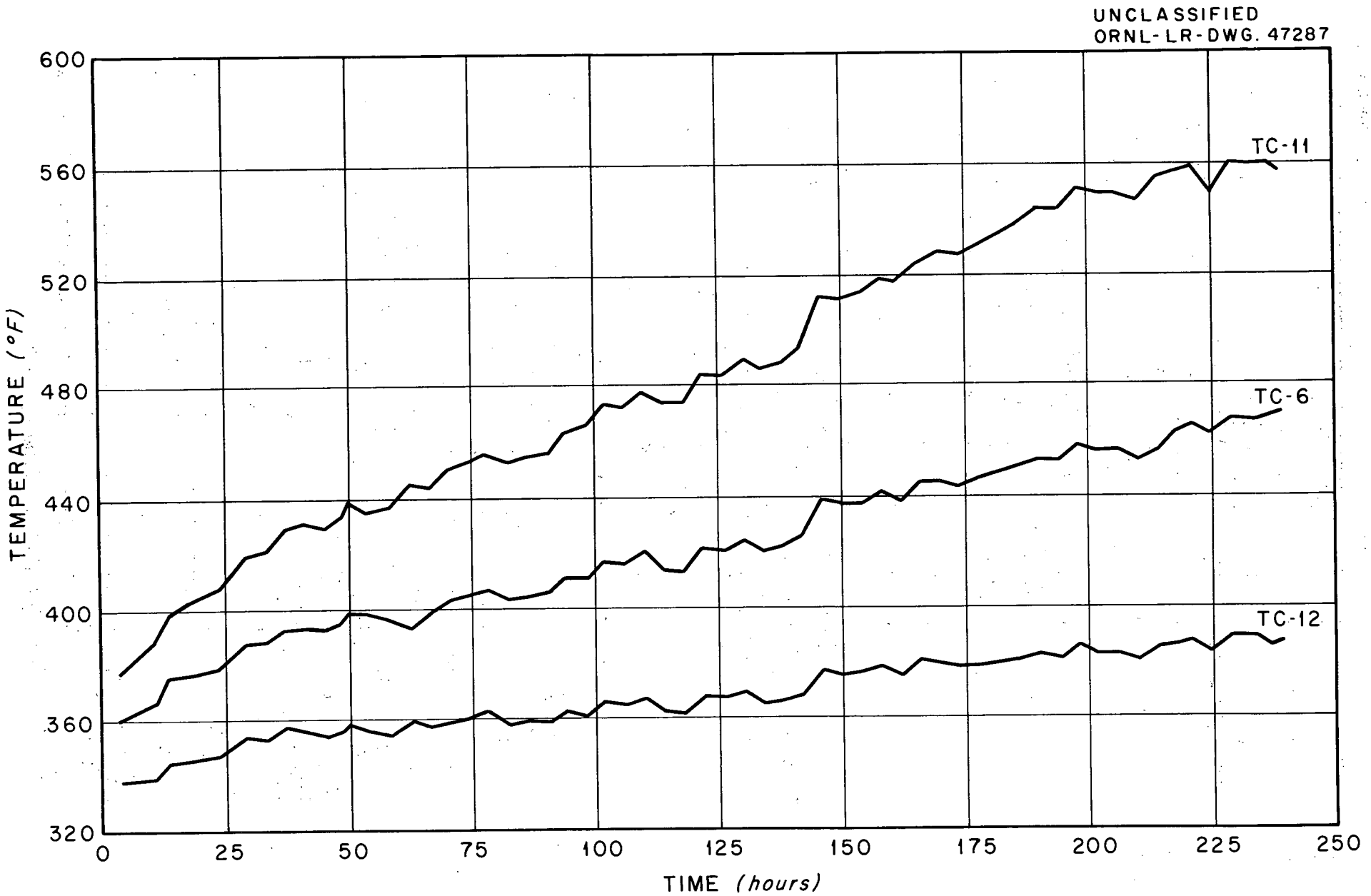

Fig. 7. Temperature Along the Test Specimen During Test. Thermocouples 12, 6 and 11.

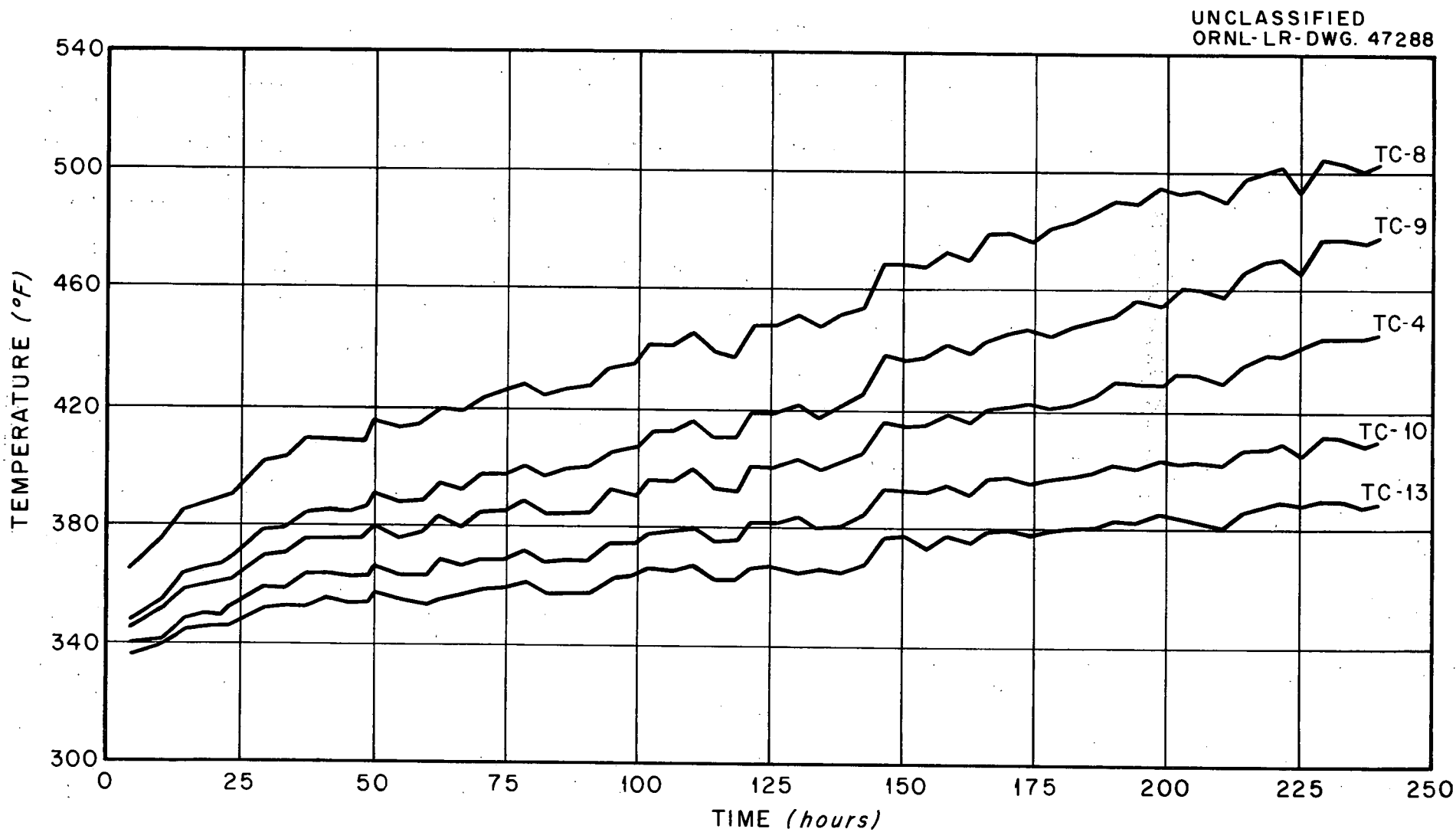

Fig. 8. Temperature Along the Test Specimen During Test. Thermocouples 13, 10, 4, 9 and 8.

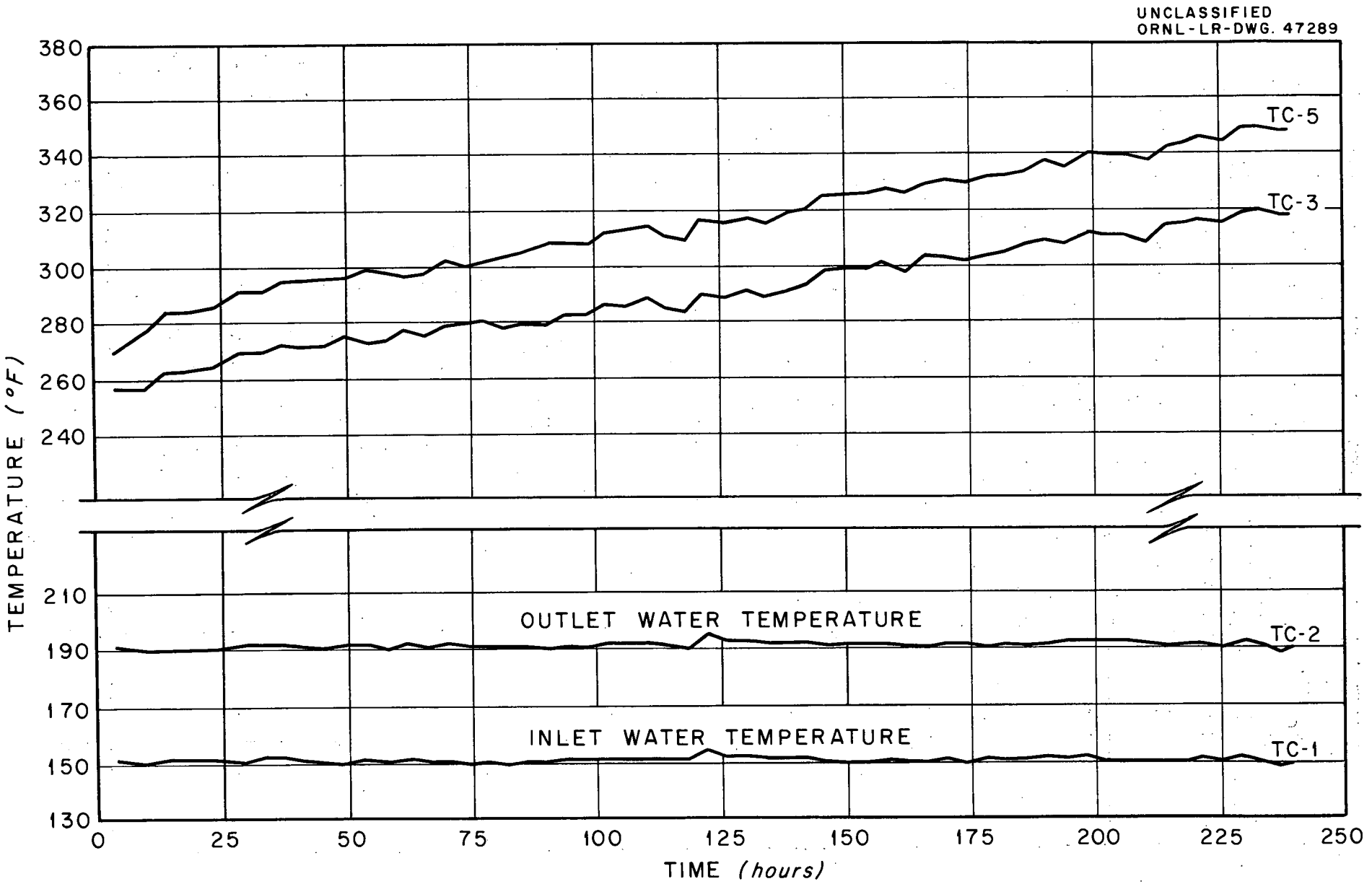

Fig. 9. Temperature on the Sides of the Test Speciman (Thermocouples 3 and 5) and of the Inlet and Outlet Water (Thermocouples 1 and 2) During Test.

varied during this period. As shown in Figs. 7, 8, and 9, all temperatures after a fairly rapid initial rise continued to increase at a somewhat reduced constant rate for the duration of the test, except those at thermocouple locations 8 and 11 which appeared to level off at 504 and 561°F, respectively, near the end of the test.

Water Chemistry

Aliquots of the water circulating in the loop were removed periodically for pH and electrical conductivity determinations. Table 3 shows the water quality at various times during the run. At the start of the run the conductivity of the water increased, but after about a day the bypass ion exchanger had decreased the conductivity to near its original value; as the run progressed the conductivity decreased still further. Chemical analyses of the water were not made, and the reason for the increased conductivity at the start of the run is not known.

Table 3. Water Conditions During the 10-Day Test

Time from Start of Run (hr)	Conductivity (micromhos)	pH
0	1.6	6.3
6.5	4.3	7.0
7.5	3.6	7.2
23.8	1.5	7.3
25.8	0.91	6.5
72.3	1.6	6.3
95.9	1.2	6.2
145.5	0.98	6.2
169.2	0.91	6.2
192.0	0.77	6.6
216.2	0.77	6.5
240.0	1.6	6.3

Heat Balance

During the run the flow rate of water through the test piece, the inlet water temperature, and the outlet water temperature were recorded; all remained essentially constant at 2.95 gpm, 155°F, and 192°F, respectively. At the start of the test the current through the test piece was 9800 amp, and the voltage drop over the test section was 1.70 v. During the test there was a slight decrease in current and a corresponding increase in voltage drop, so that the total power generation in the test section remained nearly constant at 55,000 Btu/hr·ft^2 (16 kw). Table 4 shows the agreement between the measured electrical input and the water heat-balance determinations made during the run. The total heat generated in the test specimen was very close to the design value. Considering the errors inherent in the measurements involved, the agreement between the water and electrical heat balances was excellent, indicating that heat loss other than to the water was less than 5% of the total heat input. With the particular geometry and coolant surface area of the specimen, a heat input of 55,000 Btu/hr·ft^2 corresponded to a heat flux across the surface of the thicker portion of the specimen of 1.62×10^6 Btu/hr·ft^2 and to 0.50×10^6 Btu/hr·ft^2 across the remainder of the surface.

Specimen Examination

Change in Electrical Resistance

At the conclusion of the run the test assembly was removed from the loop and its electrical resistance was re-measured. A value of 1.15×10^{-4} ohm was obtained, compared with a value of 1.10×10^{-4} ohm at the beginning of the test. Whether this is a significant difference

is not known, but an increase in electrical resistance would be expected as a result of corrosion.

Table 4. Heat Generated in the Test Specimen as Calculated from Electrical Input and from Loop Heat Balance

Time (hr)	Current (amp)	Voltage Drop (v)	Calculated Heat Input (Btu/hr) From Electrical Input	Calculated Heat Input (Btu/hr) From Heat Balance
4.1	9800	1.70	56,900	55,400
29.1	9740	1.72	57,200	54,700
53.6	9620	1.71	56,100	54,200
78.2	9500	1.72	55,800	54,800
102.2	9520	1.74	56,500	54,500
126.0	9380	1.72	55,100	56,600
150.7	9520	1.80	58,500	53,300
174.0	9440	1.81	58,300	54,200
198.3	9460	1.83	59,100	54,800
225.2	9400	1.84	59,000	55,300
239.2	9340	1.82	58,000	54,700

Visual Examination

After the electrodes were cut from the aluminum test section, the edges were carefully milled off so that the test section could be opened for examination of the coolant channel. Figure 10 is a photograph of the coolant channel showing the appearance of the surface exposed to the water. The locations of the thermocouples (except Nos. 3 and 5, which were located at mid-length on the thin low-heat-flux sections) are indicated on the photograph. The parallel marks, perpendicular to the length of the specimen shown in Fig. 10, are the result of fabrication and are not related to corrosion.

UNCLASSIFIED
ORNL-LR-DWG. 47290

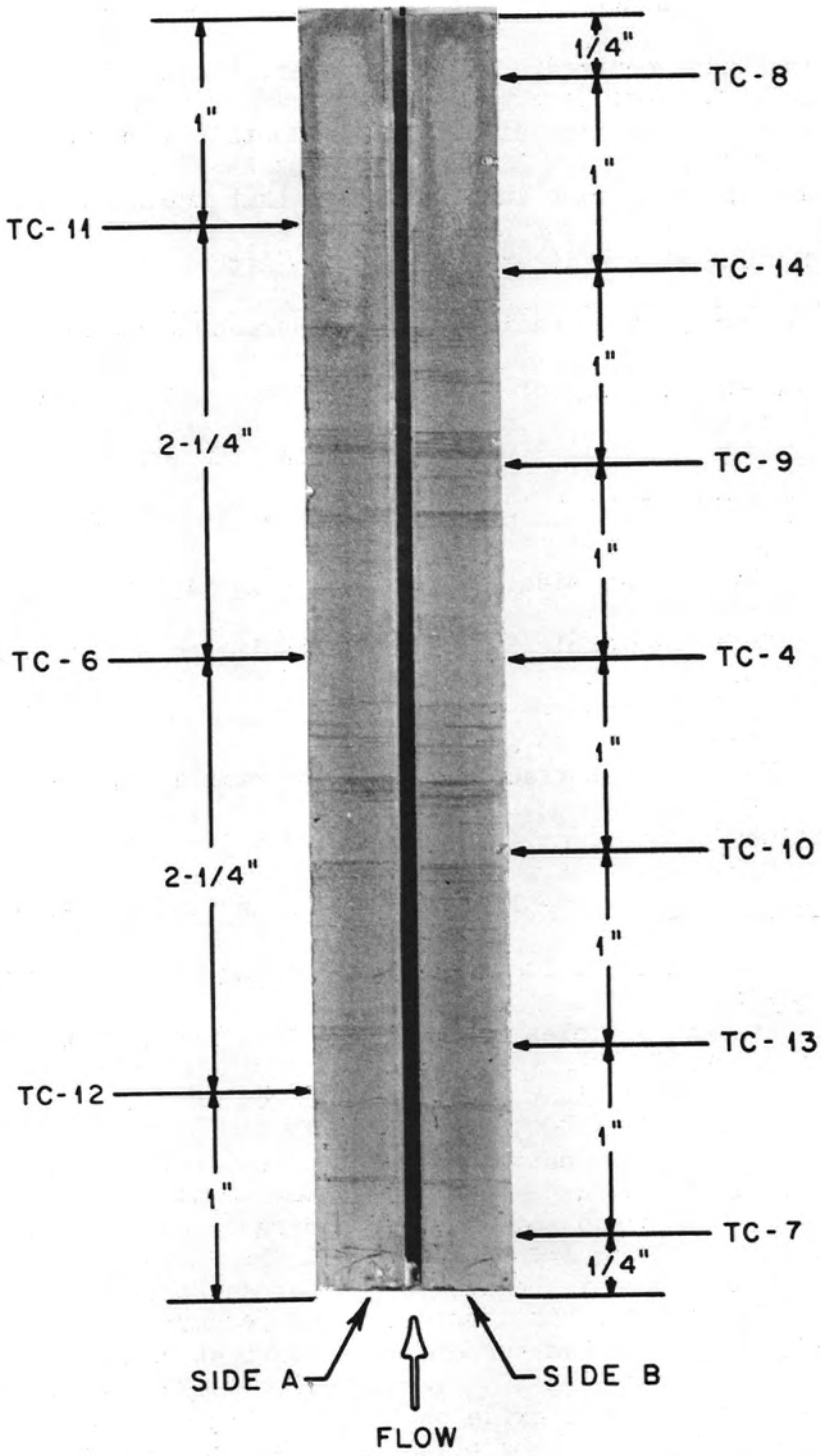

Fig. 10. Photograph of the Test Specimen at the End of the Test.

The interior surfaces of both halves of the test section appeared to be free of oxide except near the outlet where some obvious attack or "film-stripping" had occurred. As shown later, the metallic appearance was deceptive since this area did, in fact, contain a substantial oxide deposit. From the photograph it can be seen that the length of the region showing the obvious attack is greater on side A than on side B. Although a direct comparison of the readings of the thermocouples on opposite sides cannot be made because of different thermocouple location, an examination of Figs. 7, 8, and 9 shows that the temperatures were generally higher on side A (containing thermocouples 11, 6, and 12), indicating a higher heat flux on that side. Side A was slightly larger in cross section than side B (see Table 5) and as a result had a higher power generation.

The remainder of the surface appeared essentially unaffected except for some localized pitting, at least a part of which was attributable to the fabrication procedure. Small particles of an iron-containing alloy seemed to have been embedded in the surface during the forming operation; during the test these particles corroded and left pits, in the bottoms of which was a red deposit that was probably iron oxide.

Under microscopic examination it was apparent that all surfaces had been roughened and contained some tightly adherent, nearly transparent, glassy oxide; the areas near the outlet (hotter end that had a "film-stripped" appearance) that had suffered the heaviest corrosion damage contained a nonuniform, white oxide on top of a tightly adherent oxide. Figure 11 is an enlarged photograph of the surface near the outlet, showing the irregular nature of the deposit at this location. Figure 12

shows a similar enlargement of the surface directly under thermocouple 4, which was located mid-way between inlet and outlet. For comparison, Fig. 13 is a photograph of the surface of an unexposed test piece fabricated in exactly the same manner as the one tested. The surface appearance shown in Fig. 12 was typical of all the surfaces except that part near the outlet. The degree of roughening increased from inlet to outlet as shown later (see Table 5).

Table 5. Thickness of Each Side of the Test Piece and Surface Roughness at the End of the Test

Distance from Outlet (in.)	Thickness (in.) Side A	Thickness (in.) Side B	Surface Roughness* (μin.)
0	0.0990	0.0990	ND**
1/2	0.1015	0.0970	50-60
3/4	0.1020	0.0975	
1 1/4	0.1025		30
2	0.1030	0.0970	
2 1/2	0.1032	0.0965	
3	0.1035	0.0970	40
4	0.1039	0.0967	
4 5/8	0.1038	0.0970	ND**
6	0.1025	0.0970	20
6 1/2	0.1005	0.1000	

* Root-mean-square values over the length indicated.

** Not determined.

UNCLASSIFIED
ORNL-LR-DWG. 47291

Fig. 11. A Photograph of the Surface of the Test Specimen Near the Outlet. Mag. 23X.

UNCLASSIFIED
ORNL-LR-DWG. 47292

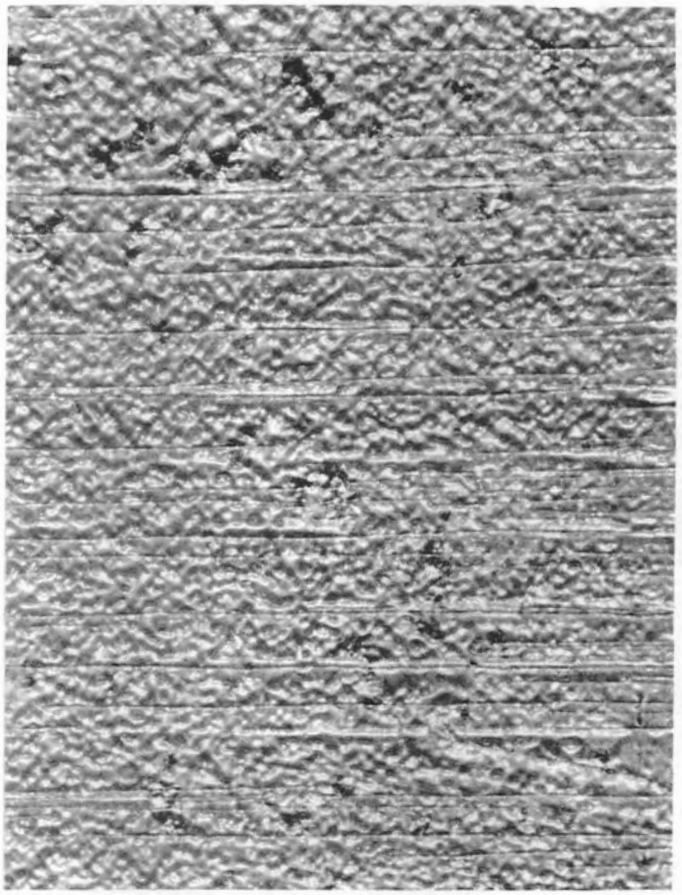

Fig. 12. A Photograph of the Surface of the Test Specimen Directly Under Thermocouple 4. Mag. 23X.

UNCLASSIFIED
ORNL-LR-DWG. 47293

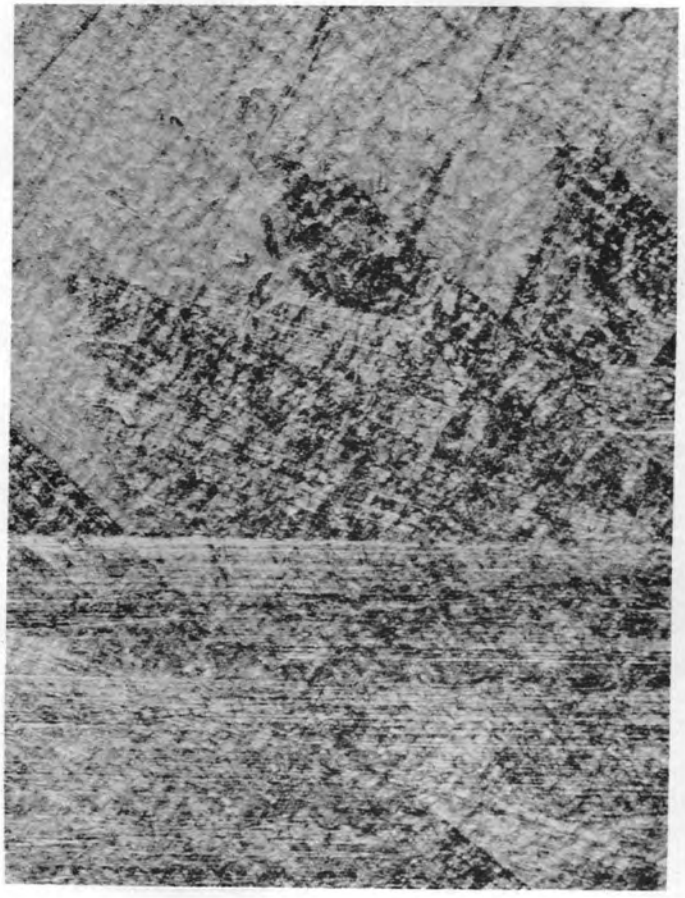

Fig. 13. A Photograph of the Surface of an Unexposed Specimen. Mag. 23X.

Specimen Thickness and Surface Roughness

The thickness of each half of the specimen was measured at several points along the length, and surface roughness determinations were made at several locations. All measurements were made on the specimen in the "as-removed" condition. The surface roughness measurements were made with a diamond stylus profilometer, calibrated to read roughness in root-mean-square microinches. Table 5 shows the results. Comparison of column 2 with column 3 in Table 5 shows that side A was about 5% thicker than side B, and since the power generation is directly proportional to the cross section, the heat flux was approximately 5% greater on side A. Thus the corrected heat fluxes during the test were 1.66×10^6 Btu/hr·ft^2 on side A and 1.58×10^6 Btu/hr·ft^2 on side B, assuming no conduction of heat to the thin, lower-temperature side sections. This fact probably explains why side A was hotter and corroded to a greater extent than side B.

Determination of Oxide Thickness

Half of the specimen, side B, was cut into six pieces, each about 1 in. long, as shown in Fig. 14. After carefully removing burrs and using steel wool to remove metal deposits at sites where thermocouples had been attached, the thickness was determined with a micrometer at the locations indicated on the sketch and each piece was weighed. The oxide was then electrolytically removed[2] and the measurements were repeated. Table 6 shows the thickness of oxide as determined by each method. To calculate the average oxide thickness from weight-change data, the density of the aluminum oxide was assumed[9] to be 4 g/cm^3. The film thicknesses determined by the two methods are not in close agreement. Some

UNCLASSIFIED
ORNL-LR-DWG. 47294

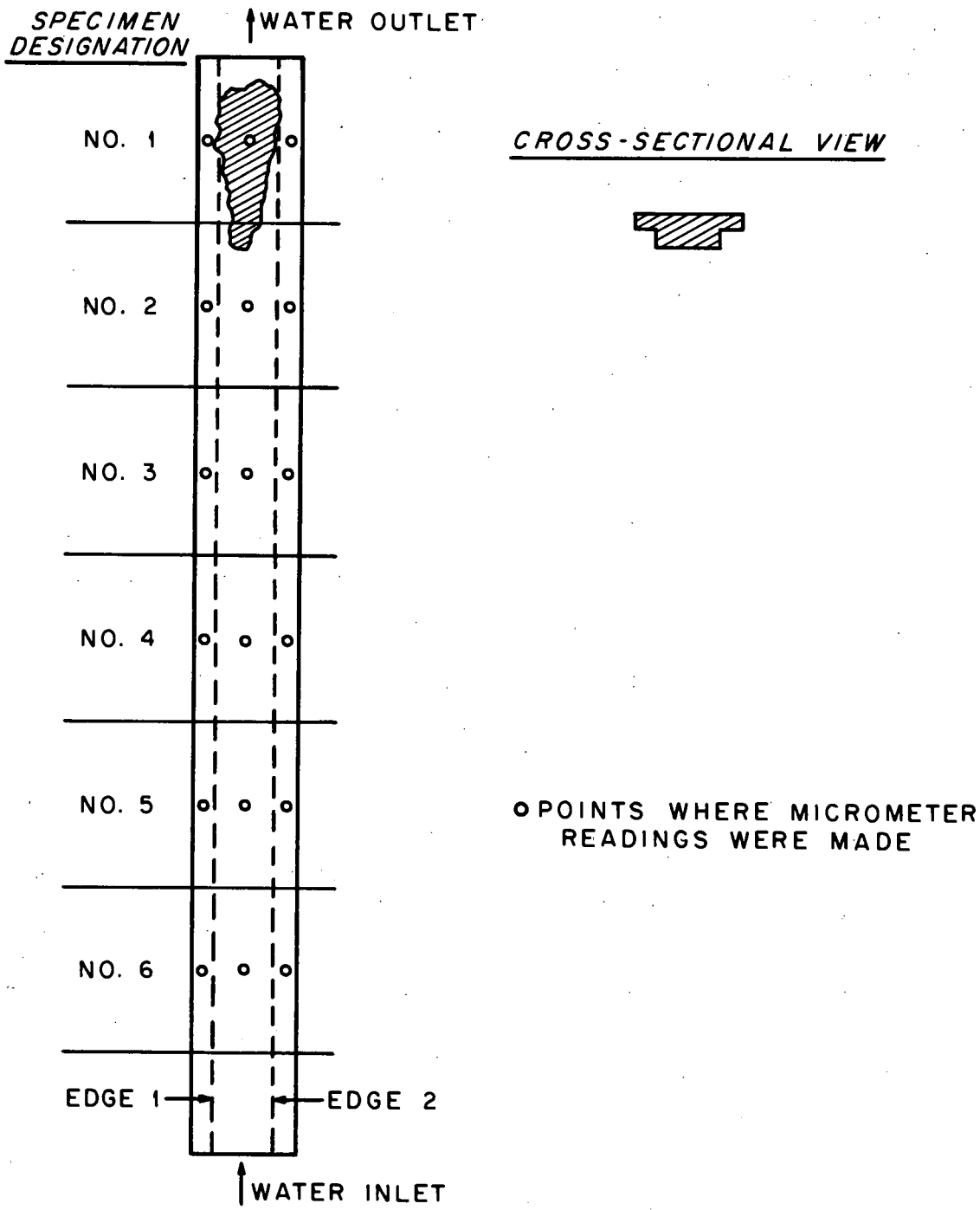

Fig. 14. Schematic Drawing of Half of Test Specimen Showing Locations of Sections and Points at Which Micrometer Measurements Were Made.

difference in thickness values would be expected between the two methods because of the nonuniform nature of the surface deposit; however, the magnitude of the difference was greater than expected. Although the absolute values of film thickness as determined by the two methods disagree, both methods show that oxide thickness increased from inlet to exit.

Table 6. Thickness of Aluminum Oxide on Side B of Test Specimen

Specimen Designation	Thickness of Aluminum Oxide (mils)			
	By Micrometer Measurement			By Weight Change
	Edge 1	Center	Edge 2	Average for Specimen
1	2.0	3.0	1.5	0.70
2	1.5	2.0	2.5	0.79
3	3.0	2.0	1.5	0.71
4	0.5	2.0	1.0	0.54
5	1.5	1.5	1.0	0.51
6	1.0	1.5	0.5	0.34

A small amount of the corrosion-product oxide was carefully scraped from an unused portion of the specimen and subjected to x-ray diffraction examination. Only $\alpha \cdot Al_2O_3 \cdot H_2O$, boehmite, was detected. Since this is the same oxide observed on aluminum surfaces corroded by high-temperature water, the heat flux did not alter the composition of the corrosion product.

Metallographic Examination

The second half of the test section, side A, was sectioned at 1-in. intervals along its length, starting at 0.5 in. from the outlet end. These sections were mounted in Bakelite, polished, and etched for

metallographic examination. Figure 15 shows the type of attack observed at a distance of 0.5 in. from the outlet in the region of maximum attack (see Fig. 10 for orientation). Intergranular attack to a depth of 0.005 in. is clearly evident in the photomicrograph. Figure 16 shows the photomicrograph of a similar section 1.5 in. from the outlet in the region where the heavy attack had just started. In this region the depth of intergranular attack was only about 0.001 in.; slight surface roughening is also apparent. At both locations intergranular attack was found only in the center region of the specimen where the heat flux was highest; the edge surfaces where the heat flux was lower were completely free of localized attack. The other four sections showed no evidence of intergranular attack, regardless of heat flux, and the surface roughness of the metal was similar to that shown in Fig. 12. Thus only in the region where "film-stripping" had occurred was there evidence of intergranular attack.

In the photomicrographs shown in Figs. 15 and 16, the oxide on the surface is not discernible because of the technique used in printing the photomicrograph. However, the oxide on all surfaces is evident in Fig. 17, which shows cross-sectional views at six different locations along the length of the test piece on side A. The irregular oxide thickness and the cracks and imperfections in the oxide are clearly visible. The general surface condition of the aluminum can also be seen.

On each of the six sections cut from side A, the oxide thickness on the surface was measured across the full 0.500-in. width of the specimen in the following manner: Starting at one edge of the specimen, the

UNCLASSIFIED
ORNL-LR-DWG. 47295

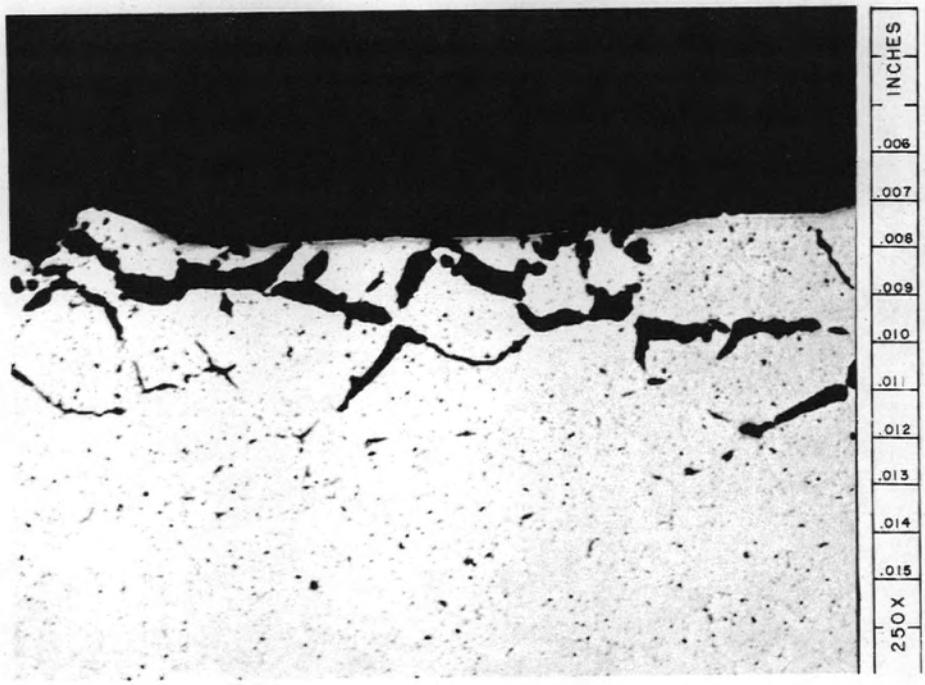

Fig. 15. Photomicrograph Showing the Extent of Intergranular Attack 0.5-in. from Outlet of Specimen. Mag. 250X.

UNCLASSIFIED
ORNL-LR-DWG. 47296

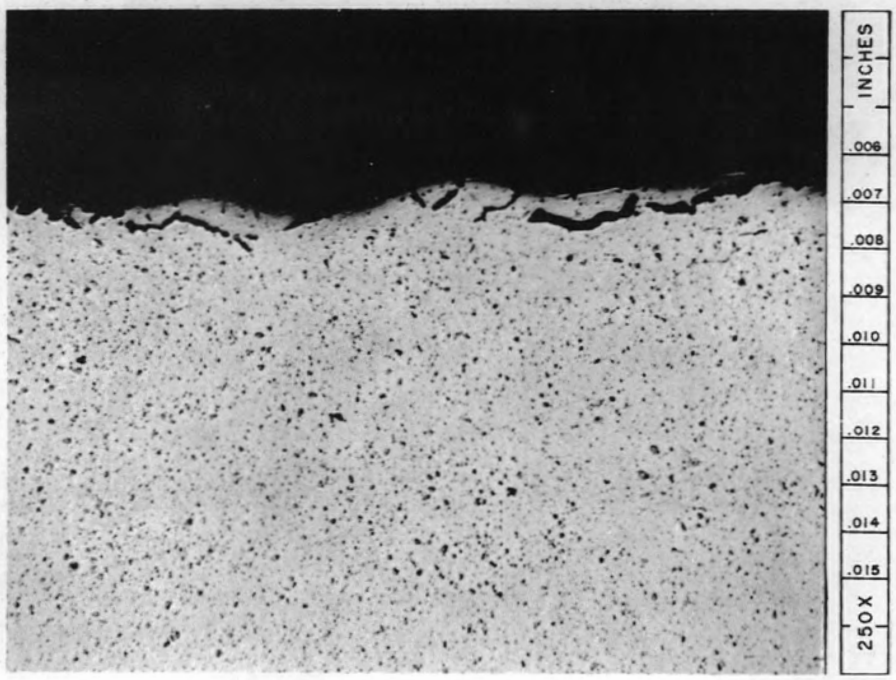

Fig. 16. Photomicrograph Showing the Extent of Intergranular Attack 1.5-in. from Outlet of Specimen. Mag. 250X.

UNCLASSIFIED
ORNL-LR-DWG. 47297

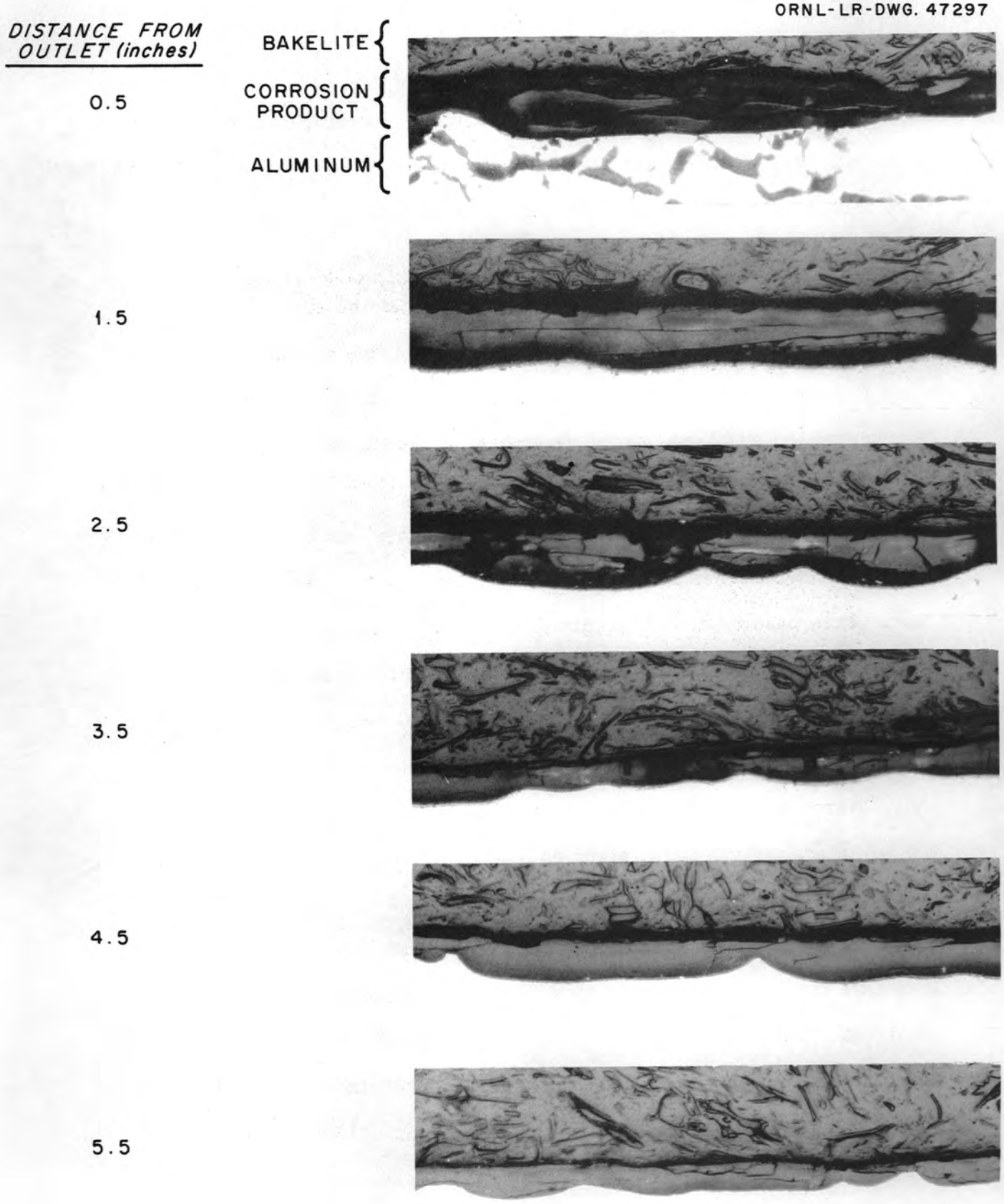

Fig. 17. Photomicrographs Showing the Corrosion Products on the Aluminum Surface at Various Locations Along the Test Specimen. Mag. 250X.

microscope was adjusted so that the diameter of the field of vision was 1 mm. In this field the minimum and maximum oxide thicknesses were measured. The specimen was then moved so that the same measurements were made in the next 1-mm field and so on across the piece. Since the width of the specimen was approximately 12 mm, 12 minimum and maximum thicknesses were determined on each of the six cross sections. The results are shown in Fig. 18, where the average maximum and average minimum thicknesses are plotted against the distance from the outlet. At each region examined, there were no significant differences in oxide thicknesses across the specimen, although the heat flux on the edges was 0.50×10^6 Btu/hr·ft^2, whereas that in the center was 1.66×10^6 Btu/hr·ft^2. Thus at each location the thickness of oxide was independent of the heat flux. This observation is in disagreement with the data reported in Table 6, which shows the oxide deposit to be thicker on the surface subjected to the higher heat flux. It is apparent from Fig. 17 that in most cases the area covered by the thicker oxide is much greater than that covered by the thin oxide so that an average oxide thickness would not be an average of the minimum and maximum values in Fig. 18 but would be much closer to the maximum curve.

Because of the manner of fabrication of the test section, weight-loss data or absolute changes in thickness of aluminum could not be obtained. Therefore a determination of the amount of aluminum oxidized per unit area could not be made. From unreported isothermal data obtained by the authors, it was estimated that the extent of uniform corrosion under the conditions of test would be 1 to 2 mils. From the above photographs it is apparent that intergranular penetration amounted to a

UNCLASSIFIED
ORNL-LR-DWG. 47298

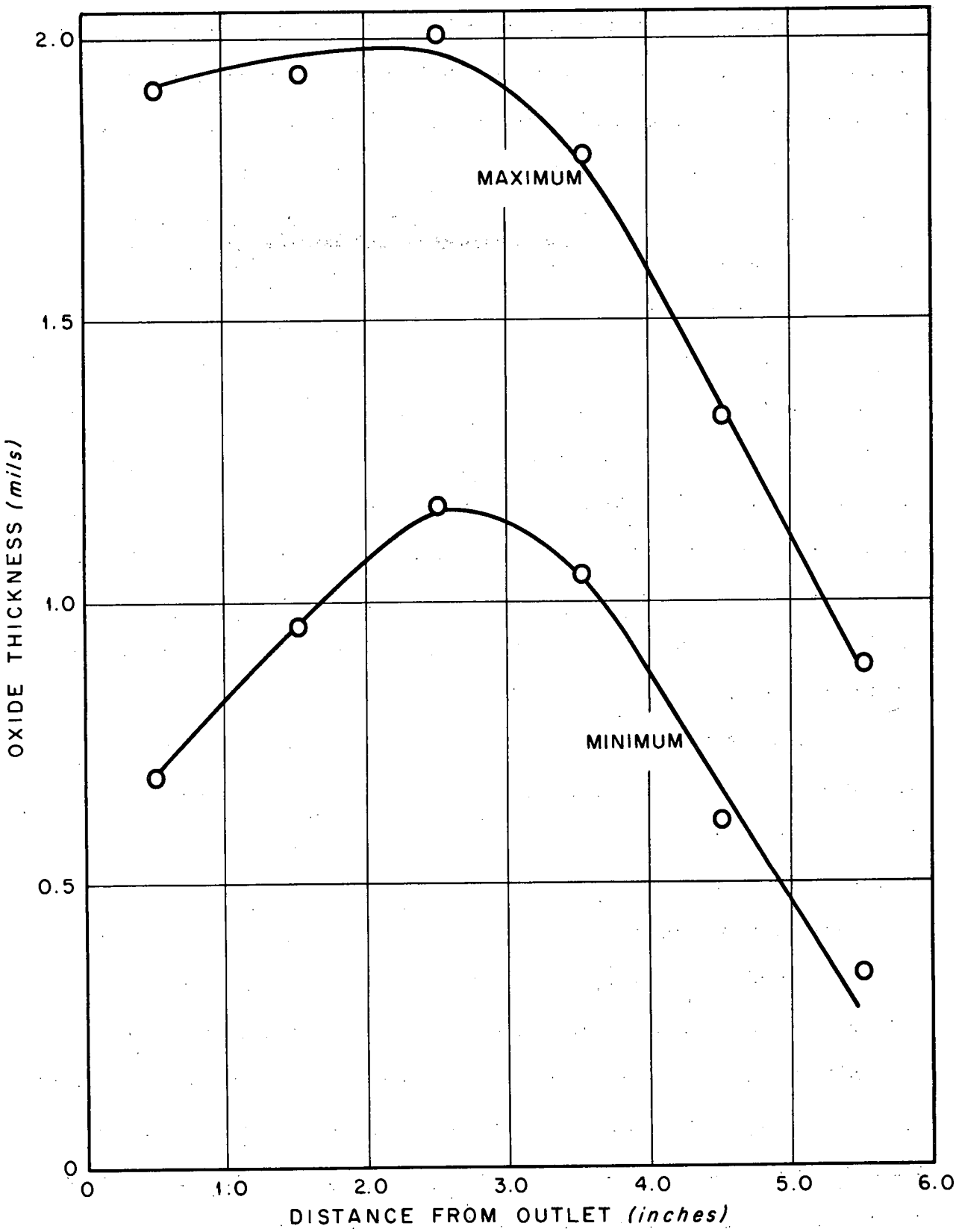

Fig. 18. Thickness of Corrosion Products on Side A of Test Specimen as Determined Metallographically.

maximum of 5 mils. If 2 mils of general attack is added to the localized attack, 7 mils is obtained as the best estimate of the maximum total penetration of the aluminum during the 10-day test.

DISCUSSION

The equipment used in this experiment functioned well. Temperatures were easily maintained within ±1 to ±2°F of the desired value, and variations in flow rates and pressure were negligible. As already shown, the heat input to the test specimen was constant within about ±3% during the 10-day test. The versatility designed into the system and the demonstrated reliability indicate that the equipment will be most useful in investigating the effect of heat flux on the corrosion of aluminum or other metals over wide ranges of variables.

The results of this first test indicate that the use of 1100 aluminum as cladding for fuel elements or for heat-transfer surfaces in general can, under certain circumstances, lead to aluminum temperatures higher than might normally be expected. Certainly the formation of an insulating layer of corrosion products on the aluminum surface, as was observed in this test, would produce an effective barrier to heat transfer and lead to increased aluminum temperatures. But how well the corrosion-product layer would adhere and to what thickness it would grow was, and still is, difficult to predict. In this particular test aluminum oxide increased to a maximum thickness of about 0.002 in. It was interesting to note that at the hotter end of the test specimen the adherent oxide film may have reached a limiting thickness since some rather loose oxide was present on top of the adherent oxide, and in this region there was

at least an indication that the aluminum temperature was approaching a steady-state value.

In view of the temperature of the aluminum and the "film-stripped" appearance of both sides near the exit, a question might be raised as to whether or not boiling contributed to the "stripping." The highest temperatures recorded on the outside of the specimen were 561°F on side A (thermocouple 11) and 504°F on side B (thermocouple 8). The calculated temperature drop through the aluminum was 51°F for side B and 57°F for side A, the difference being due to slightly different thicknesses and heat fluxes on the two sides. Thus, if water could penetrate the oxide through cracks or pores, it would come in contact with aluminum at 504°F on side A and 453°F on side B. The saturation pressures corresponding to these temperatures are 705 psia and 436 psia, respectively. Since the pressure at the exit of the test specimen was constant between 345 and 395 psia (uncertainty in accuracy of pressure gage), it is possible that boiling could have occurred if water penetrated to the aluminum - aluminum oxide interface during the latter stages of the test and that boiling might have influenced the stripping. Future experiments will be conducted to see if "film-stripping" is related to boiling.

Only in the "film-stripped" region did the aluminum show evidence of intergranular attack. The presence of this type of attack was unexpected, since the highest possible temperature of the aluminum in contact with water was 504°F (at thermocouple 11). Several unreported isothermal tests conducted at 500°F, during which 1100 aluminum was exposed to water at flow rates of 20 to 65 fps for 10-day periods,

indicated no intergranular attack. Why the aluminum suffered intergranular attack in this test where the time in contact with 500°F water was only 2 to 3 days and whether this attack was attributable to an effect of heat flux cannot be answered at this time.

If it is assumed that the amount of oxide on the surface of the aluminum at the start of the test was insignificant, it is possible to calculate a temperature for any point on the test specimen. These calculations were carried out for each of the thermocouple locations, and the calculated temperatures are compared with the observed temperatures in Table 7. The water film coefficient at each location was calculated by means of the Sieder-Tate equation, and the temperature drop through the metal was calculated considering uniform heat generation throughout the metal and heat removal from one side.

The agreement between calculated and observed temperatures is good, except at thermocouple locations 3 and 5 which were in the area of low heat flux (thin edges). Apparently the reason the temperatures at these locations were substantially higher than calculated was because of the conduction of heat from the adjoining high-temperature region. Thus the heat flux on the thin cross section may have been somewhat higher than calculated and that on the 0.100-in.-thick section, somewhat lower.

In the present test the specimen had been used during calibration of the loop and electrical system prior to the beginning of the test during which time some corrosion products undoubtedly formed on the aluminum. This fact could have caused the measured temperatures to be higher than those calculated on the assumption that the aluminum surface was free of oxide.

Table 7. Comparison of Calculated and Observed Temperatures on the Outside of the Aluminum Test Specimen at the Beginning of the Test

Thermocouple Number	Calculated* Temperature (°F)	Observed Temperature (°F)
7	343	**
12	350	338
13	345	336
10	345	340
4	349	345
6	354	360
9	354	347
14	356	**
11	360	378
8	355	368
3	213	257
5	213	266

* The calculated temperatures take into account the slight variation in wall thickness and consequently heat flux between the two sides.

** Not measured.

The thermal conductivity of the oxide film may be calculated from the measured oxide thickness and the temperature increase during the test. Table 8 shows the thermal conductivity values obtained at the three thermocouple locations on side A, using both the minimum and maximum oxide thicknesses determined metallographically (Fig. 18) and the temperature rise observed during the 10-day test (Fig. 7). Using the minimum oxide thickness of Fig. 18, values ranging between 0.5 and 1.0 Btu/hr·ft^2·°F/ft are obtained; using the maximum oxide thickness, values between 1.4 and 2.4 are obtained. The reliability of these values may be subject to question, but the values are of the order of magnitude expected.

Table 8. Thermal Conductivity of the Corrosion-Product Oxide Calculated from Temperature Difference Across the Oxide and Measured Oxide Thicknesses

Thermocouple Number	Measured Temperature (°F)		Δt (°F)	Oxide (mils)		Thermal Conductivity (Btu/hr·ft²·°F/ft)	
	Initial	Final		Max.*	Min.**	Max.	Min.
11	378	567	189	1.9	0.7	1.4	0.5
6	360	469	109	1.8	1.0	2.3	1.3
12	338	388	50	0.9	0.4	2.4	1.0

* Taken from the upper curve in Fig. 18.

** Taken from the lower curve in Fig. 18.

Although the results of only one test are always subject to question, the data obtained under conditions simulating those proposed for the fuel region of the High-Flux Isotope Reactor indicate that the corrosion of 1100 aluminum is severe and that undesirably high temperatures can be expected in the fuel elements unless some means can be found to reduce the quantity of oxide formed on the heat-transfer surface. Since the quantity of oxide formed is proportional to the corrosion of aluminum, inhibiting the corrosion of aluminum should result in a decrease in metal temperature. Future tests will be concerned with determining the effectiveness of inhibitors compatible with the rest of the High-Flux Isotope Reactor system and with a determination of the corrosion resistance of other aluminum alloys.

ACKNOWLEDGMENTS

The authors wish to express their appreciation to L. A. Haack for assistance in design of the test specimen, to P. G. Herndon, Jr., for design and installation of instrumentation, and to M. T. Kegley for metallographic examination of the test specimen.

REFERENCES

1. J. E. Draley and W. E. Ruther, "Aqueous Corrosion of Aluminum, Part I," Corrosion 12, 441t-448t (1956).
2. J. E. Draley and W. E. Ruther, "Aqueous Corrosion of Aluminum, Part II," Corrosion 12, 480t-490t (1956).
3. J. E. Draley et al., "High-Temperature Aqueous Corrosion of Aluminum Alloys," Proceedings of the Second UN International Conference on the Peaceful Uses of Atomic Energy, Geneva 1958, P/714, Vol. 5, p 113-120, United Nations, New York (1958).
4. K. Videm, "Corrosion of Aluminum with Additions of Iron and Silicon in High-Temperature Water," Proceedings of the Second UN International Conference on the Peaceful Uses of Atomic Energy, Geneva 1958, P/767, Vol. 5, p 121-127, United Nations, New York (1958).
5. H. Coriou et al., "Al-Fe-Ni Alloys Corrosion Resistant in Hot Water," Proceedings of the Second UN International Conference on the Peaceful Uses of Atomic Energy, Geneva 1958, P/1271, Vol. 5, p 128-152, United Nations, New York (1958).
6. J. A. Ayres et al., "High-Temperature Aqueous Corrosion of Aluminum Alloys," Proceedings of the Second UN International Conference on the Peaceful Uses of Atomic Energy, Geneva 1958, P/1430, Vol. 5, p 153-156, United Nations, New York (1958).

7. J. A. Ayres, private communication, August 1959.

8. T. E. Cole, High-Flux Isotope Reactor: A General Description, ORNL CF-60-3-33 (Mar. 15, 1960).

9. M. D. Ferrier, Minutes of Conference on the Corrosion of Aluminum in Water at High Temperature Held at Chalk River, Ontario, CR-Met-700, p 7 (June 1957).

ORNL-2939
Reactors-General
TID-4500 (15th ed.)

INTERNAL DISTRIBUTION

1. HRP Director's Office Rm. 259, Bldg. 9204-1
2. S. E. Beall
3. A. M. Billings
4. D. S. Billington
5. E. G. Bohlmann
6. S. E. Bolt
7. J. R. Brown
8. W. D. Burch
9. C. E. Center
10. R. H. Chapman
11. R. A. Charpie
12. R. S. Cockreham
13. E. L. Compere
14. F. L. Culler
15. D. G. Davis
16. R. J. Davis
17. O. C. Dean
18. D. M. Eissenberg
19. L. B. Emlet (K-25)
20. J. L. English
21. D. E. Ferguson
22. C. H. Gabbard
23. W. R. Gall
24. J. P. Gill
25-44. J. C. Griess
45. W. R. Grimes
46. P. A. Haas
47. P. H. Harley
48. C. S. Harrill
49. P. N. Haubenreich
50. J. W. Hill
51. E. C. Hise
52. H. W. Hoffman
53. A. Hollaender
54. G. H. Jenks
55. W. H. Jordan
56. P. R. Kasten
57. G. W. Keilholtz
58. M. J. Kelly
59. C. P. Keim
60. M. T. Kelley
61. J. A. Lane
62. C. G. Lawson
63. S. C. Lind
64. R. S. Livingston
65. R. A. Lorenz
66. M. I. Lundin
67. R. N. Lyon
68. W. L. Marshall
69. T. H. Mauney
70. H. F. McDuffie
71. R. E. Moore
72. R. L. Moore
73. C. S. Morgan
74. J. P. Murray (Y-12)
75. K. Z. Morgan
76. L. F. Parsly, Jr.
77. M. L. Nelson
78. F. N. Peebles
79. M. L. Picklesimer
80. J. L. Redford
81. S. A. Reed
82. W. D. Reel
83. P. M. Reyling
84. D. M. Richardson
85. R. C. Robertson
86. M. W. Rosenthal
87. H. C. Savage
88. D. Scott, Jr.
89. C. H. Secoy
90. E. D. Shipley
91. M. D. Silverman
92. M. J. Skinner
93. A. H. Snell
94. I. Spiewak
95. J. A. Swartout
96. A. Taboada
97. E. H. Taylor
98. D. G. Thomas
99. M. Tobias
100. W. E. Unger
101. G. M. Watson
102. A. M. Weinberg
103. C. E. Winters
104-105. Reactor Experimental Engineering Library
106-107. Central Research Library
108-127. Laboratory Records Department
128. Laboratory Records, ORNL R.C.

129-130. ORNL - Y-12 Technical Library, Document Reference Section
131. G. M. Adamson
132. R. D. Cheverton
133. J. E. Cunningham
134. L. A. Haack
135. P. G. Herndon
136. T. M. Kegley
137. P. Patriarca

EXTERNAL DISTRIBUTION

138. D. H. Groelsema, AEC, Washington
139. Division of Research and Development, AEC, ORO
140-723. Given distribution as shown in TID-4500 (15th ed.) under Reactors-General category (75 copies - OTS)